



2016 IEEE MTT-S International Microwave Symposium (IMS)

An optically transparent analog frontend for a solar powered 24 GHz RFID transponder

Q. H. Dao
B. Lüers
T. T. Ngo
B. Geck

Suggested Citation:

Q. H. Dao, B. Lüers, T. T. Ngo, and B. Geck. An optically transparent analog frontend for a solar powered 24 GHz RFID transponder. In *2016 IEEE MTT-S International Microwave Symposium (IMS)*, pages 1–4.

Digital Object Identifier (DOI): [10.1109/MWSYM.2016.7539991](https://doi.org/10.1109/MWSYM.2016.7539991)

This is an author produced version, the published version is available at <http://ieeexplore.ieee.org/>

©2017 IEEE Personal use of this material is permitted. Permission from IEEE must be obtained for all other uses, in any current or future media, including reprinting/republishing this material for advertising or promotional purposes, creating new collective works, for resale or redistribution to servers or lists, or reuse of any copyrighted component of this work in other works.

An Optically Transparent Analog Frontend for a Solar Powered 24 GHz RFID Transponder

Q. H. Dao, B. Lüers, T. T. Ngo and B. Geck
Institut für Hochfrequenztechnik und Funksysteme
Leibniz Universität Hannover
Hannover, Germany
dao@hft.uni-hannover.de

Abstract—This paper presents an optically transparent analog frontend of an RFID transponder which is suitable for integration on a solar cell. First, insertion losses of different configurations of microstrip lines (MS) and ground plane made of grid lines are discussed. With these knowledge a meshed analog frontend consisting of a modulator and a demodulator unit is developed. Its optical transparency is determined to 85% and the electromagnetic properties are comparable to its opaque counterparts. The achieved sensitivity of the transponder is about -39 dBm input power. As low power consumption is of major interest, a discussion on the energy requirements of the used components is carried out. A prototype is realized to evaluate the simulation results.

Index Terms—RFID, Internet of Things, K-band, optical transparency, photovoltaic cell.

I. INTRODUCTION

Radio Frequency Identification (RFID) is one of the important technologies in terms of Internet of Things. Conventionally, an RFID system consists of a reader and a transponder. In our modern world each object can be equipped with a transponder to exchange information wirelessly with other devices. Interesting parameters are for example ID number or the current status of the object during its life time. Therefore, memory and sensor systems can be integrated within a transponder. In order to power the whole unit as long as possible an efficient energy concept has to be designed. Using a solar cell is a promising approach for an unlimited energy source [1]. To design a compact sized transponder a stacked structure is considered in this contribution (see Fig. 1). In this case the digital circuitry including an ultra-low power microcontroller (MCU) acting as a control unit is placed underneath the solar cell. The feed line between antenna and analog frontend should be as short as possible in order not to decrease the signal quality. Therefore, these RF structures are placed on the same layer. To integrate this configuration on the solar cell optical transparency is of great importance. There are many possibilities to realize transparent conductive strip lines [2] [3]. On the one hand transparent conducting oxides such as indium tin oxide (ITO) can be used but this material has poor conductivity [4] compared to conventional metals like copper. In addition, the reflectance, absorptance and transmittance of ITO are wavelength-dependent [4] in the usable light spectrum of the solar cell. On the other hand meshing the surface plane and ground plane of the traditional strip lines is an alternative way to achieve transparent conductive grid lines.

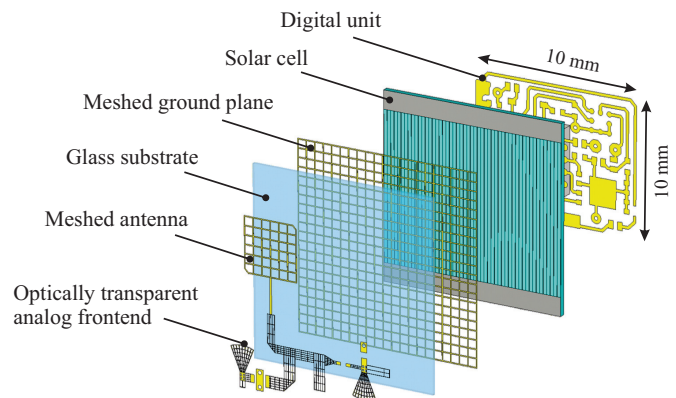


Fig. 1: Explosion view of the proposed structure of the transponder with an optically transparent antenna and analog frontend on the top layer.

Furthermore, optically transparent substrates like glass can be used as carrier material. Thus, a meshed microstrip antenna [5] and an optically transparent analog frontend are suitable for integration on a solar cell.

II. MESHED ANALOG FRONTEND

In the following section an optically transparent analog frontend is presented. Quartz glass is used as carrier material with a thickness of 0.22 mm. The dielectric constant $\epsilon'_r = 3.81$ and $\tan \delta = 0.0004$ at 24 GHz is determined by a resonator measurement method. The simulations are carried out using Ansys HFSS 2015 for the investigations of meshed microstrip lines (MMS) and Keysight Technologies Advanced Design System (ADS 2009) for the design of the meshed analog frontend.

A. Meshed Microstrip Line (MMS)

First of all, electromagnetic properties of MMS have to be investigated before designing more complex circuits. Therefore, different configurations of MMS are analyzed concerning their insertion losses since they have a major impact on the signal quality. In this consideration the line impedance plays a minor role. An example of an MMS consisting of five horizontal grid lines is depicted in Fig. 2. The grid line width w_l is set to 0.01 mm for all configurations, while the horizontal and vertical distances d_h , d_v and d_{vg} (vertical distance of

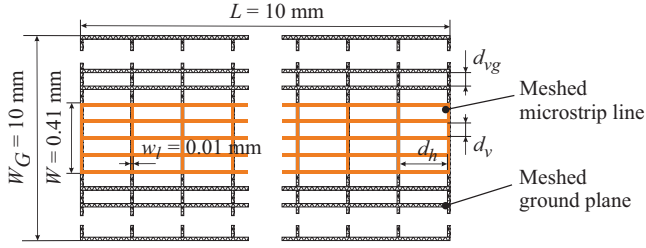
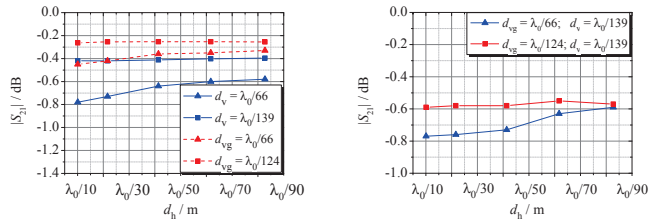


Fig. 2: Layout of a meshed microstrip line (MMS with five horizontal grid lines) over a meshed ground plane.



(a) MMS over opaque ground plane (solid lines); opaque MS over meshed ground plane (dashed lines) (b) MMS over meshed ground plane

Fig. 3: Simulated insertion losses of different MS configurations.

the ground plane) are varied. The thickness of both copper layers is assigned to $1\ \mu\text{m}$ since the intended RF sputtered metal coatings are in this range of thickness. Fig. 3a shows the simulation results of MMS over an opaque ground plane (solid lines) and opaque MS over a meshed ground plane (dashed lines), respectively. It can be noted that a variation of the vertical distance d_v causes a higher impact on the insertion losses than a change in the horizontal space d_h . Fig. 3b illustrates the insertion losses due to meshing both the MS and the ground plane. Depending on the selection of grid spaces a variation of $\pm 0.13\ \text{dB}$ can be observed for the studied configurations. All values are evaluated at $24\ \text{GHz}$ ($\lambda_0 = 12.5\ \text{mm}$). For comparison an insertion loss of $0.14\ \text{dB}$ can be observed for a conventional microstrip line with the same width and length.

B. Modulator and Demodulator

The proposed design of a meshed modulator and demodulator circuit is depicted in Fig. 4. All grid line widths are about $0.01\ \text{mm}$. Some pads are not meshed due to the attachment of components on them as well as the realization of vias. The horizontal and vertical spaces between the grid lines are designed in a manner in order to minimize the insertion losses of the MMS. In addition, the optical transparency has to be considered too. Thus, the meshed ground plane area underneath the MMS has more grid lines than the region further away from the actual structure. According to this design the overall transparency is about 85% (based on an area of $10 \times 4.4\ \text{mm}^2$) which is determined by the simulation software Zemax OpticStudio 15.5.

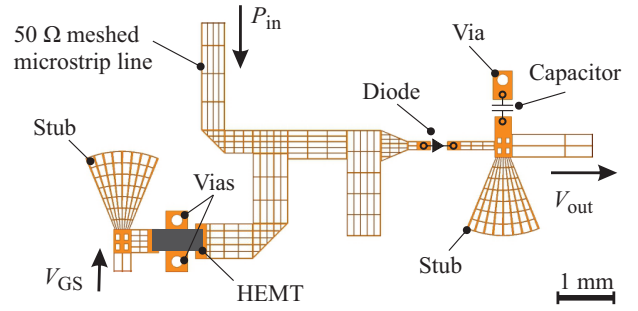


Fig. 4: Layout of the proposed meshed analog frontend; top: component side; bottom: ground plane.

As power efficiency is of major interest, backscattering based on amplitude shift keying (ASK) is used for the data transfer from the transponder to the reader unit. The communication distance d between these units can be calculated as follows [6]:

$$d^4 = \frac{P_T G_R^2 \lambda_0^4 G_{\text{Tag}}^2}{P_R (4\pi)^4} |\Gamma_1 - \Gamma_2|^2 \quad (1)$$

where P_T is the transmitted power of the reader, P_R is the received power at the reader, G_R is the gain of the reader antenna, G_{Tag} is the gain of the transponder antenna and λ_0 is the free space wavelength. The performance of backscattering is mainly determined by two realized reflection states Γ_1 (mismatched case) and Γ_2 (matched case), assuming all other variables remained constant. In order to generate these two states an Avago VMMK-1225 high electron mobility transistor (HEMT) is used in a common source configuration. The drain is connected to the microstrip line while the source is routed to the ground plane. The gate is connected to a microcontroller which controls the transistor by switching the voltage on ($V_{\text{GS}} = 0.7\ \text{V}$) and off ($V_{\text{GS}} = 0\ \text{V}$). In this way backscattering can be realized. The usage of a HEMT offers low power consumption ($6.3\ \mu\text{W}$ @ $0.7 V_{\text{GS}}$) and a good backscatter modulation performance [7].

For the reception of the reader's commands an envelope detector is realized by a Keysight HSCH-9161 zero bias beam lead Schottky diode and a $0.3\ \text{pF}$ capacitor from Johanson Technology. The two stubs (see Fig. 4) are responsible for decoupling the microwave and the baseband signal. The MMS are designed in a manner to meet the required impedance

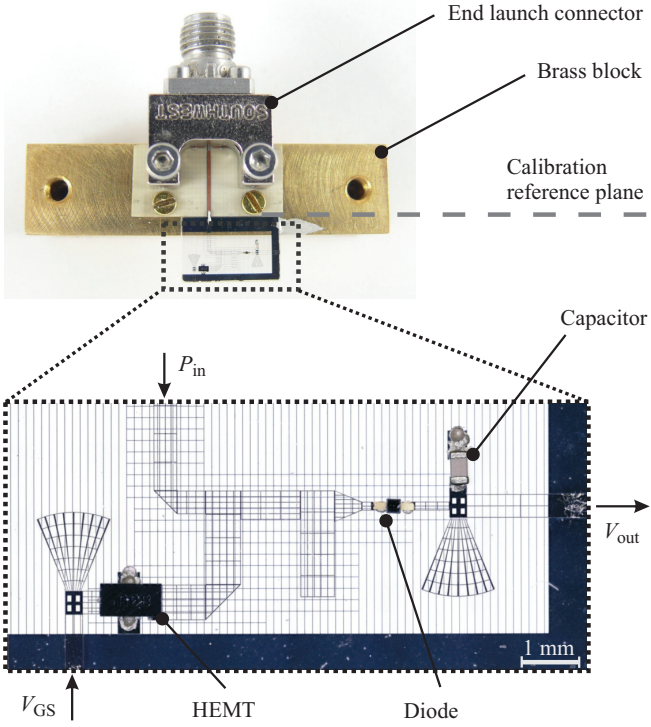


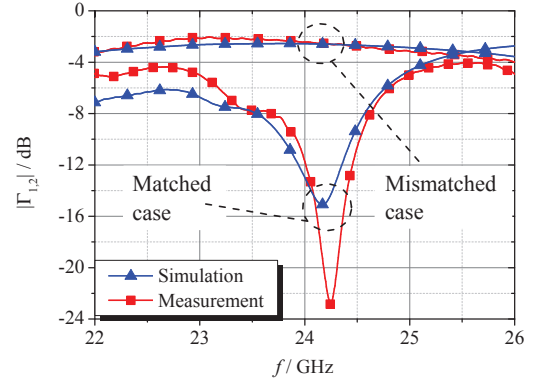
Fig. 5: Picture of the realized prototype on quartz glass; top: measurement setup; bottom: detailed view of the meshed analog frontend with electronic components bonded by two-component adhesives.

matching between the modulator and demodulator circuit and the $50\ \Omega$ microstrip line which can be connected to an antenna or to an end launch connector for measurement purposes.

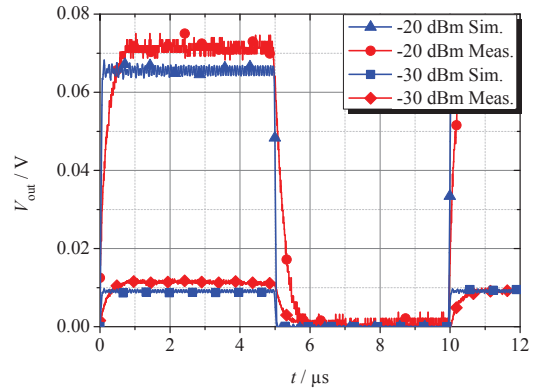
C. Realization and Verification

The optically transparent analog frontend fabricated on a quartz glass is shown in Fig. 5. The top and bottom side consist of three different metal layers ($0.05\ \mu\text{m}$ chromium, $1\ \mu\text{m}$ copper and $0.3\ \mu\text{m}$ platinum) with an overall thickness of approx. $1.3\ \mu\text{m}$. To obtain the ground connections for the transistor and the capacitor through glass vias are produced by laser ablation. Afterwards, the glass substrate is RF sputtered. As a result reliable conductive vias can be achieved. The MMS and the meshed ground plane are realized by the subsequent ion beam etching process. As shown in Fig. 5 the fabricated glass substrate is fixed on a block made of brass for measurement purposes. A RO4003C laminate is used to bond the MS of the PCB and the MMS of the analog frontend. A TRL calibration process is utilized to de-embed the influence of the end launch connector.

Fig. 6a depicts the simulated and measured input reflection coefficients of the analog frontend for two different states at an input power of $-20\ \text{dBm}$. The curves marked with triangles represent the simulated data and the curves marked with squares are measurement results. There is a slight shift of about $70\ \text{MHz}$ (corresponding to 0.29%) concerning the



(a) Input reflection coefficients at $-20\ \text{dBm}$ input power



(b) Demodulated envelope

Fig. 6: Simulated and measured input reflection coefficients for the two transistor switching states and demodulated envelope of the realized prototype.

resonance frequency for the matched case. All in all, a good agreement can be obtained for both switching states. At the frequency of $24\ \text{GHz}$ the measured reflection coefficients are $-2.4\ \text{dB}$ and $-12\ \text{dB}$, respectively.

Since a data rate of $100\ \text{kbit/s}$ is desired for the communication between the reader and the transponder, an incident wave is modulated with a $100\ \text{kHz}$ rectangular signal to obtain the envelope. Fig. 6b shows the simulation results of the demodulated envelopes for two different input power values. At an input power level of $-30\ \text{dBm}$ the measured amplitude of the envelope is $11\ \text{mV}$ and the rectangular waveform still remains unchanged. A good agreement between simulation and measurement is achieved. The mismatch concerning the slope of the envelope is caused by the measurement setup and mainly by the input capacitance of the oscilloscope.

These demodulated signals can be conducted to a comparator that converts the output voltage of the detector to logic level. Thus, a simple decoding with a microcontroller (MCU) is possible. In [7] a low power comparator was used (LMV7271 from National Semiconductor; $16.2\ \mu\text{W}$ @ $1.8\ \text{V}$) which needs at least $30\ \text{mV}$ signal level to detect the

right data. In order to decrease the threshold voltage and thus extending the communication range, another comparator (TS3021 from STMicroelectronics) is evaluated in this work. The result shows a threshold level of 3 mV corresponding to an incident power of $P_{in} = -37$ dBm, but in contrast this component has a higher power consumption ($126 \mu\text{W}$ @ 1.8 V). Further improvement concerning threshold level, energy demand and component reduction can be achieved by using the internal comparator of an MCU from Texas Instruments (MSP430FR5738). The investigation shows a minimal sensitivity value of -39 dBm with simultaneous reduction in power consumption ($58 \mu\text{W}$ @ 2 V). This value is verified by a measurement with the realized prototype.

III. POWER CONSUMPTION

To meet the criteria of low power consumption of the transponder the aforementioned ultra-low power MCU is used. Since it is a central management unit its energy requirement should be well known. Therefore, a communication example (request for the current temperature value) between the reader and the transponder and the corresponding current consumption are shown in Fig. 7. The measured voltage signal (blue curve) is recorded at the output of the demodulator while the voltage V_{GS} of the transistor is represented by the green curve. It can be noted that the request from the reader occurs within the first 0.22 ms. Due to the processing time of the MCU the response of the transponder has a delay of approx. 0.64 ms. The red curve in Fig. 7 represents the current consumption for a supply voltage of 2 V during a communication sequence. It can be seen that the time varying current consumption can be divided into six states:

- State 1: The MCU is in standby mode (approx. 0.033 mA). This operation mode should be optimized to reduce power consumption as most of the time the transponder is in the standby mode.
- State 2: The MCU changes its state of operation to active as it receives a request from the reader. In this case a request for the current temperature value.
- State 3: In this state the request is processed by the MCU. The current can be measured to approx. 0.8 mA.
- State 4: The A/D converter is activated for measuring the temperature value.
- State 5: The MCU transmits the requested data by switching the gate source voltage V_{GS} on and off.
- State 6: At the end of the communication procedure the MCU switches back to standby mode.

IV. CONCLUSION

This contribution presents the design of an optically transparent analog frontend made of grid lines. Meshed microstrip lines are investigated concerning its insertion losses by varying the grid space. Compared to a conventional microstrip line the results show an additional attenuation up to 0.6 dB for the studied configurations. Based on these findings an 85 % optically transparent modulator and demodulator circuit consisting of a transistor, a diode and a capacitor is investigated. By means

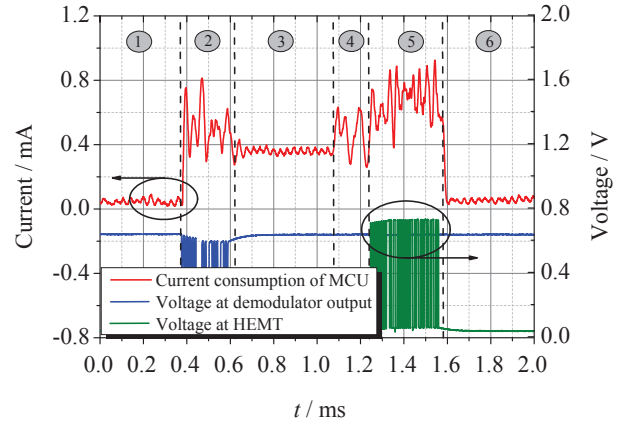


Fig. 7: Communication flow of a reader request for the current temperature value and the current consumption of the MCU.

of an efficient ultra-low power microcontroller the power consumption varies between $58 \mu\text{W}$ and 1.85 mW and the overall sensitivity of the proposed transponder is determined to -39 dBm incident power. A prototype is realized and the measurements show a good agreement with simulated results.

ACKNOWLEDGMENT

The authors wish to thank the German Research Foundation for the financial support in the framework of the Collaborative Research Center 653. Furthermore, the authors wish to thank Ms. Lisa Jogschies and Mr. Philipp von Witzendorff for their efforts in producing the structures on glass substrate.

REFERENCES

- [1] J. Meyer, Q.H. Dao, and B. Geck, "24 GHz rfid communication system for product lifecycle applications", 2nd International Conference on System-Integrated Intelligence: New Challenges for Product and Production Engineering (SysInt), 2014.
- [2] J.R. Saberlin and C. Furse, "Challenges with Optically Transparent Patch Antennas", *IET Microw. Antennas Propag.*, vol.8, Iss.13, pp.1091-1096, 2014.
- [3] J. Hautcoeur, L. Talbi, K. Hettak, and M. Nedil, "60 GHz optically transparent microstrip antenna made of meshed AuGI material", *Antennas and Propagation Magazine, IEEE*, vol.54, no.8, pp.10-16, June 2012.
- [4] D. S. Ginley, *Handbook of transparent conductors*, New York: Springer Science+Business Media, 2010.
- [5] Q.H. Dao, T. J. Cherogony and B. Geck, "Optically Transparent and Circularly Polarized Patch Antenna for K-Band Applications", 10th German Microwave Conference (GeMiC), 2016.
- [6] P.V. Nikitin, K.V.S. Rao, and R.D. Martinez, "Differential RCS of RFID Tag", *Electronics Letters*, vol.43, no.8, pp.431-432, April 2007.
- [7] J. Meyer, Q.H. Dao, and B. Geck, "Design of a 24 GHz analog frontend for an optically powered RFID transponder for the integration into metallic components", 43rd European Microwave Conference (EuMC), 2013.